6-2008

# Synthesis And Characterization Of Type II ZnSe/CdS Core/Shell Nanocrystals

Alexander Nemchinov

Maria Kirsanova

Nishshanka N. Hewa-Kasakarage

Mikhail Zamkov
*Bowling Green State University*, zamkovm@bgsu.edu

# Synthesis and Characterization of Type II ZnSe/CdS Core/Shell Nanocrystals

**Alexander Nemchinov, Maria Kirsanova, Nishshanka N. Hewa-Kasakarage, and Mikhail Zamkov***

*The Center for Photochemical Sciences and Department of Physics, Bowling Green State University, Bowling Green, Ohio 43403*

*Received: February 20, 2008; Revised Manuscript Received: April 13, 2008*

High-quality ZnSe/CdS core/shell nanocrystals, exhibiting a type II carrier localization regime, were fabricated via a traditional pyrolysis of organometallic precursors. The two-step synthesis involved fabrication of 4.5−6 nm ZnSe seeds followed by a subsequent deposition of the CdS shell. An efficient spatial separation of electrons and holes between the core and the shell was observed for heterostructures containing more than three monolayers of CdS, which was primarily evidenced by the spatially indirect emission tunable from 480 to 610 nm for a fixed core diameter. Because of a large (type II) offset of band edges at the core/shell interface, fabricated nanocrystals exhibited a relatively low spectral overlap between emission and absorption profiles, with associated Stokes shifts of up to 110 nm. The quantum yield of as-prepared samples was 12−18% and was further improved to 20% after purification of nanocrystals through multiple hexane/methanol extractions. Novel properties of synthesized ZnSe/CdS nanocrystals as well as their applicability to practical realizations in areas of biomedical imaging, solar sells, and quantum dot-based lasers are discussed.

## Introduction

Combining two or more semiconductor materials in a single heterojunction quantum dot (QD) facilitates the design of nanocrystals with adjustable electronic and optical properties, leading to the fabrication of novel materials for technological applications that include solar cells,[1–3] biolabeling,[4] and QD-based lasers.[5–7] Recently, considerable progress was made in the synthesis of type II heterojunction nanostructures that spatially separate photoexcited electrons and holes in different parts of a composite QD. These core/shell nanocrystals are made of two semiconductor materials with a particular alignment of conduction and valence band edges at the interface, which creates a step-like radial potential favoring the localization of one of the carriers in the core of a QD and the other one in the shell. The resulting charge separation leads to a strong dipole moment, indirect band gap radiative emission, and a large offset between absorption and emission spectral profiles. It is thought that these fascinating properties would facilitate the use of QDs in several technological applications including photovoltaics, where spatial charge separation can increase the light conversion efficiency, biomedical labeling where the low overlap between emission and absorption energies of the dye eliminates the cross-talk phenomena, and QD-based lasers, where photoinduced electric dipole across the type II QD Stark shifts the biexciton level, resulting in a desirable linear amplification regime.

Several combinations of semiconductor materials have been used thus far to fabricate type II core/shell nanocrystals, including CdTe/CdSe,[8] CdTe/CdS,[9] CdTe/CdSe,[10] ZnTe/CdS,[11] ZnTe/CdTe,[12] CdSe/ZnSe,[13,14] and CdS/ZnSe.[15,16] Most of these heterostructures contain tellurium, which is known to have a relatively high rate of oxidation. This often leads to poor chemical stability and, thus, lowers the typical values of quantum yield (QY) for unpassivated QDs to <10%. Although the reaction of Te ions with radicals in the QD environment can be partly inhibited by adding an external layer of a wide band gap semiconductor, which increases the yield to 10−30%,[10] the use of Te-based nanocrystals in practical applications requiring high emission efficiencies and good photostability may still be encumbered. Recent synthetic efforts, therefore, turned to Te-free compounds, and a few reports on highly fluorescent CdSe/ZnSe and CdS/ZnSe type II nanocrystals (QY: CdSe/ZnSe −90%[14] and CdS/ZnSe up to 30%[15]) have appeared. The CdS/ZnSe heterojunction was particularly attractive due to a highly efficient charge separation across the interface. In these nanocrystals, the lower situated edge of the CdS conduction band led to an almost complete localization of photoinduced electrons in the core, and the higher positioned valence band of ZnSe favored the localization of holes in the shell.

While the CdS/ZnSe heterostructure is expected to have an efficient electron−hole (e−h) separation for a minimal shell thickness,[15] the reverse nanocrystal order, ZnSe/CdS, enhances other vital electronic properties and could be of even greater interest to a number of specific practical realizations. For instance, shell localization of an excited electron in ZnSe/CdS QDs will be more suitable for catalytic electron transfer in dye sensitized solar cells, as it increases the oxidation rate of $TiO_2$ in ZnSe/CdS + $TiO_2$ conjugates. Furthermore, the slightly wider band gap of the core-situated ZnSe semiconductor should result in a larger offset between absorption and emission energies of the core/shell heterostructure, which is an important feature in the development of photoluminescence (PL) biolabels. Finally, the reverse ZnSe/CdS heterojunction, where the wider band gap material is encapsulated inside a smaller band gap shell, should exhibit a somewhat greater tunability of emission colors for a fixed core size.

In the present study, we report the synthesis of ZnSe/CdS type II nanocrystals via traditional pyrolysis of organometallic precursors. The two-step synthesis involved growth and purification of ZnSe QDs followed by deposition of a CdS shell. The QY of as-prepared nanocrystals was in the range of 12−18% and was slightly improved after purification procedures (up to 20%). Upon deposition of the CdS shell onto 5.0 nm

* Corresponding author. E-mail: zamkovm@bgsu.edu.

10.1021/jp801523m CCC: $40.75 
Published on Web 06/04/2008

ZnSe seeds (size estimated from a ZnSe emission peak using ref 17), the fluorescence (FL) emission of heterostructured QDs red-shifted from 480 to 610 nm, while the main absorption edge remained near its original value measured in ZnSe QDs (410 nm). The emission wavelength was further extended into the range of 460−630 nm by using different sizes of starting ZnSe cores (4.5−6 nm). We noticed that for all fabricated combinations of shell/core sizes, the spectral overlap between absorption and emission profiles was relatively low, which is characteristic of spatially indirect carrier recombination. Several methods were employed to study the dynamics of shell deposition and to characterize the composition of the fabricated nanocrystals. Model calculations, based on the approach developed in ref 18, were used to estimate the minimal diameter of the shell needed for an efficient spatial separation of e−h wave functions inside the heteronanocrystal.

## Experimental Procedures

**Synthesis of ZnSe Seeds.** All reactions were conducted under argon atmosphere using standard Schlenk techniques. Synthesis of monodisperse wurtzite ZnSe nanocrystals was based on a procedure described in ref 19, as follows. A total of 0.3794 g (0.6 mmol) of zinc stearate was dissolved in 9.5 mL (3.2 g) of octadecane (ODA) by heating reagents to 300 °C in the 25 mL three-necked flask, while stirring. After the mixture became clear, a selenium stock solution, prepared by dissolving 0.0474 g (0.6 mmol) of selenium in 1.5 mL of trioctylphosphine (TOP), was swiftly injected into the reaction flask. During nanocrystal growth, the temperature was kept at 280 °C. The reaction was stopped after 12−22 min, depending on the desired nanocrystal size, by removing the flask from the heating mantle.

**Purification of ZnSe QDs.** After the reaction mixture was allowed to cool to 50 °C, 3−5 mL of hexane was added to the solution to prevent solidification. The subsequent cleaning of nanocrystals was performed by hexane/methanol extraction. Typically, 6−7 mL of methanol was slowly added to the reaction mixture in hexane, which was then centrifuged for 10 min at 3500 rpm. The upper yellowish hexane layer containing QDs was removed with a syringe for further purification, and the white precipitate was subjected to another hexane/methanol extraction. We found that at least three to four extraction cycles are necessary to ensure that the QY of the core/shell nanocrystals that are fabricated in the next step are maximized. Following purification procedures, a clear solution of nanoparticles in hexane was obtained. The suspension was then placed under argon and stored in the dark for future shell deposition.

**Overcoating with CdS.** For shell deposition, injection stock solutions were prepared at a concentration of 0.04 M in 1-octadecene (ODE). Cadmium was obtained by dissolving 0.030 g (0.24 mmol) of cadmium oxide in 0.6 mL of oleic acid (OA) and 5.4 mL of ODE in a 25 mL flask under argon by heating it to 280 °C while stirring. After the solution became clear, it was cooled to 60 °C. The sulfur injection solution was prepared from 0.0077 g (0.24 mmol) of sulfur dissolved in 6 mL of ODE by heating the mixture to 200 °C under argon flow. For continuous shell deposition, both precursors were mixed together and injected into a reaction vessel containing previously prepared ZnSe nanocrystals dispersed in 1.5 g of ODA and 6.3 mL of ODE at 240 °C. The injection rate was 2 mL/h. Aliquots of the reaction mixture were taken at 7−10 min intervals for UV−vis and PL spectral characterization. For shell deposition via a successive ion layer adsorption reaction (SILAR), 0.5 mL injections of Cd and S stock solutions were made sequentially every 20 min starting with Cd ions. A total of 5 monolayers (MLs) was grown.

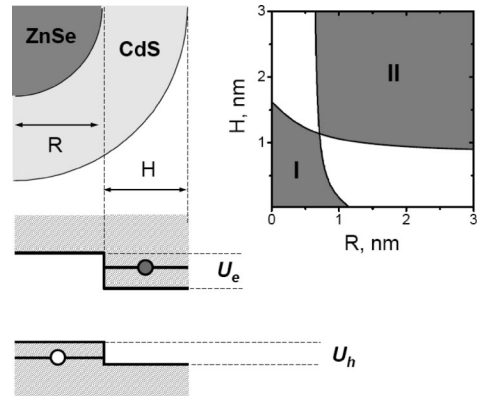


**Figure 1.** Band edge alignment at the ZnSe/CdS interface. An excited electron becomes primarily shell localized due to the lower energy of the $1S_e$ level in CdS. Similarly, the higher energy of the $1S_h$ state in ZnSe supports core localization of an excited hole. The inset contour plot shows the dependence of carrier localization regimes in ZnSe/CdS nanocrystals (either type I or type II) on the core radius, $R$, and shell thickness, $H$.

**Etching with Benzoyl Peroxide.** Controlled etching of nanocrystals with benzoyl peroxide (BPO) was performed following the technique described in refs 20and 21. Prior to etching of nanocrystals with BPO, their surface ligands were exchanged to a shorter benzylamine by placing 0.5 mL of purified ZnSe/CdS nanocrystals in hexane of a known size and concentration in ∼2 mL of benzylamine. The mixture was then sonicated for ∼15−20 min, or until the nanocrystals were totally dispersed, yielding a clear solution. A total of 1.0 mL of this suspension was added to 5.0 mL of a 3:1 toluene/methanol mixture. To initiate the etching process, a solution of benzoyl peroxide (0.165 M in 1:1 toluene/methanol) was quickly injected into the nanocrystal suspension. The etching process was monitored using an UV−vis spectrometer.

**Characterization.** UV−vis absorption and PL spectra were recorded using a Cary 50 Scan spectrophotometer and Jobin Yvon Fluorolog FL3-11 fluorescence spectrophotometer. The PL quantum yield of ZnSe/CdS nanocrystals was determined relative to quinine sulfate organic dye excited at 350 nm. X-ray spectra of purified nanocrystals deposited onto carbon substrates were measured with an energy dispersive X-ray spectrometer built into the Hitachi (S-2700) scanning electron microscope. High-resolution transmission electron microscopy measurements were carried out using a JEOL 311UHR instrument operated at 300 kV. Specimens were prepared by depositing a drop of nanocrystal hexane solution onto a Formvar-coated copper grid and letting it dry in air. XPD measurements were carried out on Scintag XDS-2000 X-ray powder diffractometer.

## Results and Discussion

**Type II Localization Conditions.** Figure 1 shows a relative alignment of the conduction and valence band edges in ZnSe/CdS heteronanocrystals. We assume that the localization of an exited electron in the shell occurs when the $1S_e$ state of CdS is energetically lower than the conduction band energy offset ($U_e$) at the core/shell interface. Similarly, a photoinduced hole is primarily localized inside a ZnSe core when the energy of the $1S_h$ state is below the valence band offset ($U_h$). Because of a strong carrier confinement in nanoscopic QDs, energy levels of an excited e−h pair strongly depend on the core radius, $R$, and the shell thickness, $H$, such that, in general, both type I

and type II localization regimes are possible for different combinations of these parameters. Here, we used known solutions to envelope-function the Schrödinger equation for noninteracting carriers,[18] to find the conditions of type II excitation character in ZnSe/CdS nanocrystals. In the present calculations, only the lowest-energy, zero angular momentum, conduction, and valence band 1S states were considered. The band structure parameters of bulk semiconductors such as effective masses ($m_e = 0.14$ and $m_h = 0.53$ for ZnSe and $m_e = 0.18$ and $m_h = 0.6$ for CdS), offset energies ($U_e = 0.8$ eV and $U_h = 0.52$ eV), and band gap energies ($E_g = 2.72$ eV for ZnSe and $E_g = 2.45$ eV for CdS) were taken from refs 22 and 23.

The contour plot in Figure 1 shows the $R$ and $H$ dependence of the localization regime in ZnSe/CdS nanocrystals. The vertical solid curve represents the $H$ dependence of minimal core radius $R_m$, for which holes become core localized, and the horizontal curve shows the $R$ dependence of minimal shell thickness, $H_m$, for which electrons are localized in the shell. In the lower left region of the plot confined by $R(H)$ and $H(R)$ boundaries in Figure 1, excited carriers are delocalized over the entire nanocrystal volume, and the optical excitations in such a heterostructure have a type I character. For large radii and shell thicknesses, $R$, $H$ is >1.2 nm, electrons and holes become primarily localized in different parts of the QD, and the type II regime is established. In present experiment, we primarily targeted the synthesis of large core quantum dots in order to minimize the amount of shell material needed to be grown to achieve type II charge separation. Accordingly, the minimal sizes of "seeding" ZnSe nanocrystals that we used for ZnSe/CdS were 4 nm.

**Steady-State Absorption and Fluorescence.** The growth of the CdS shell onto 5.0 nm diameter ZnSe seeds was monitored by taking absorption and fluorescence spectra of 0.05 mL samples from the reaction flask diluted in chloroform. The bottom spectrum in Figure 2 shows the spectral characteristics of original ZnSe seeds diluted in TOP. Both growth time and following purification procedures of ZnSe QDs were found to be critical to the final emission yield of core/shell heterocrystals (see Experimental Procedures). To ensure that ZnSe seed QDs have a well-defined absorption edge, growth times of 10−20 min were used. This resulted in the slight weakening of ZnSe FL quantum efficiency but yielded much brighter emission in the final ZnSe/CdS nanocrystals.

Growth kinetics is shown in Figures 2 and 3. Upon slow addition of Cd and S precursors to the reaction flask, the ZnSe absorption peak began to broaden, developing a low-energy tail that extended into yellow or orange for large nanocrystals. This indicates an onset of an indirect type II absorption feature, characterized by electronic transitions across the core/shell interface with energies lower than absorption of ZnSe or CdS QDs. Previous studies of type II QDs[14,15] also reported a similar broadening effect, which is proportional to the type II energy offset at the interface.

A gradual increase in the type II charge separation also is seen in the evolution of FL spectra during nanocrystal growth. The original ZnSe seed nanoparticles exhibited a fluorescence peak at 420 nm. Upon the addition of Cd and S precursors, this band quickly diminished, which is likely due to the removal of surface passivating ligands in ZnSe, while a new emission feature began to develop around 480 nm. The subsequent shell deposition is accompanied by a steady strengthening and red-shifting of this peak until it reached saturation at 605 nm. Notably, measured emission energies in ZnSe/CdS heterocrystals are smaller than those in either ZnSe or CdS QDs due to the spatially indirect character of electronic transitions across the core/shell interface. This also is evidenced by the steady increase of Stokes shifts upon shell growth that reach 100−110 nm for medium-sized nanocrystals.

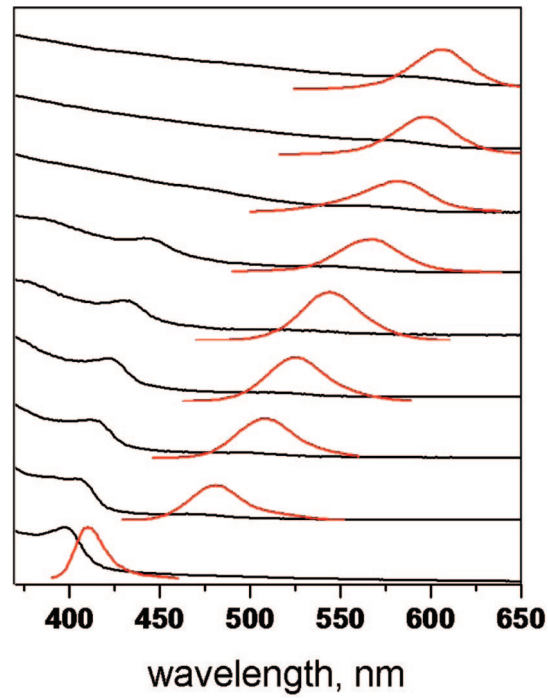


**Figure 2.** UV−vis absorption and room-temperature fluorescence spectra of ZnSe and ZnSe/CdS core/shell nanocrystals during consecutive shell growth. Bottom: spectrum of original ZnSe core QDs in TOP. Top: temporal evolution of spectral features of the growth solution showing a gradual shift of the FL peak from 480 nm (1 ML) to 605 nm (5 ML). The absorption edge of the original ZnSe cores remains centered around 420 nm.

**QY and Nanoparticle Stability.** The QY of as-prepared ZnSe/CdS nanocrystals was in the range of 12−18% and was further improved to 16−20% after extraction and purification procedures (see Experimental Procedures for details). In comparison to the QY of Te-containing type II quantum dots, the values obtained in this work were fairly high, matching those of non-Te (as-prepared) heterostructures, such as CdSe/ZnSe and CdS/ZnSe. The QY of the latter nanocrystals, for instance, composed of the same combination of semiconductor materials, was reported to be within 10−15% after purification and annealing, which is similar to the QY of unpurified nanocrystals obtained in the present study. The stability of fabricated ZnSe/CdS QDs was found to be sensitive to both the degree of purification and the number of MLs deposited during shell growth. We noticed that the PL of as-prepared nanocrystals diluted in chloroform was visibly reduced after 1 week of storage at ambient conditions in air. Purified nanocrystals showed some degree of degradation (10−20% reduction in QY) only several weeks following their synthesis when stored in the dark. Interestingly, the larger nanocrystals showed the most stability, whereas green and yellow emitting QDs were the least stable.

**Shell Growth Kinetics.** A combination of methods, including SILAR,[24] etching with benzoyl peroxide,[20] and X-ray emission analysis, were employed to evaluate the thickness of CdS shells grown on ZnSe seeds.

The core/shell structure of grown nanocrystals as well as a number of deposited MLs were first studied via controlled etching of nanocrystals with BPO.[20] This technique allows for a reduction in nanocrystal size by the gradual removal of outer

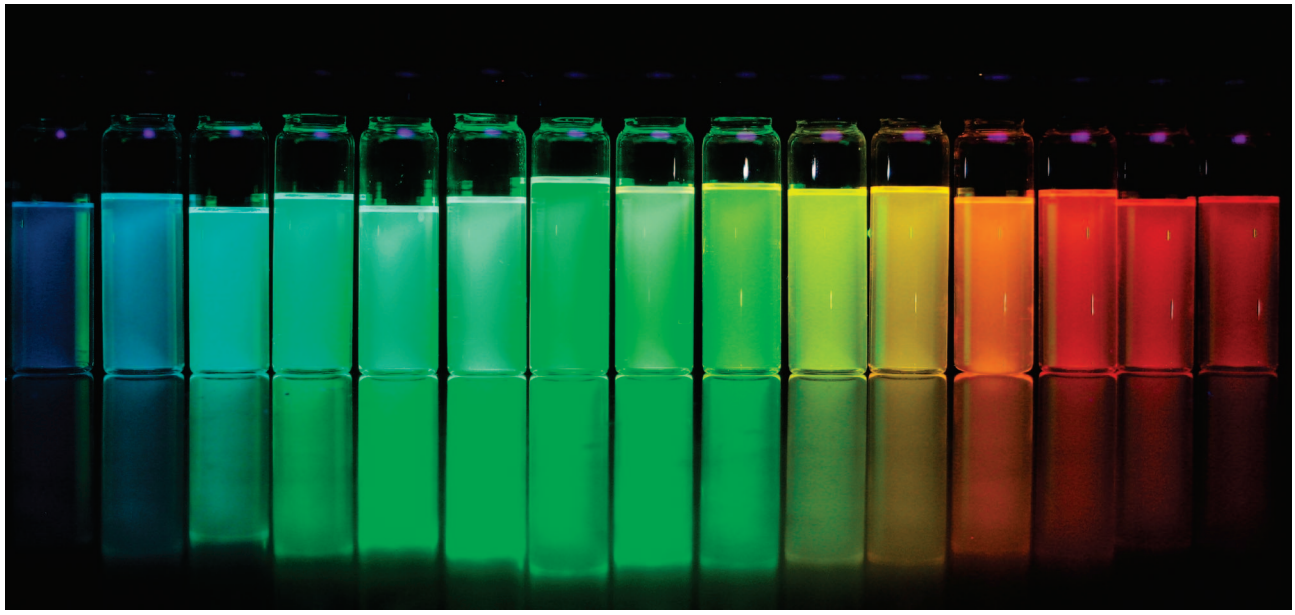

**Figure 3.** Evolution of emission colors of ZnSe/CdS nanocrystals upon continuous deposition of CdS shell.

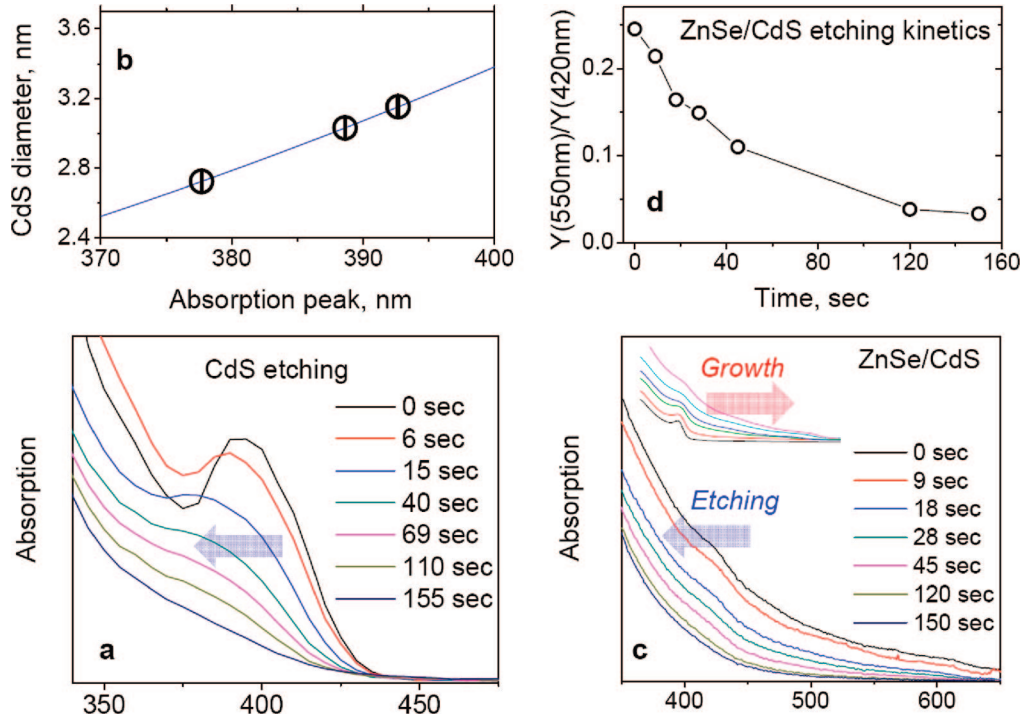


**Figure 4.** Removal of ZnSe/CdS outer shell by BPO etching. (a). Etching of a control sample of CdS QDs to determine the shell removal rate from a known association between CdS diameter and absorption peak, shown in panel b. (c) Etching kinetics of ZnSe/CdS nanocrystals showing changes in absorption spectra for different etching times. The inset shows the evolution of ZnSe/CdS absorption spectra during shell deposition. (d) Ratio of ZnSe/CdS absorption at 550 nm to absorption at 420 nm plotted vs etching time. The curve reaches saturation at 120 s, which was taken to be the total time needed for complete shell removal from ZnSe core nanocrystals.

layers, while monitoring absorption spectra in real time. Estimates of the shell thickness also can be made within this approach in a two-step procedure, where the etching rate of CdS is first measured by using a control sample of wurtzite CdS QDs with a known association of absorption peak to nanocrystal size and then used along with observed etching times of ZnSe/CdS QDs to estimate the number of CdS MLs. Because of a possible difference between the etching speed of CdS nanoparticles in the control sample and the etching speed of the CdS shell, this approach may yield larger uncertainties in determination of the shell thickness than SILAR or X-ray emission (EDX) analysis, described next. Figure 4a shows the evolution of absorption spectra of CdS nanocrystals during the etching process. Upon the addition of BPO, the original peak at 393 nm, which corresponds to band edge absorption in CdS, blue-shifts due to the reduction of nanocrystal size and then disappears completely. The first three steps in Figure 4a were used to estimate the etching rate in wavelengths per second that was subsequently converted to nanometers per second by using wavelength to size curve for CdS[25] (Figure 4b). As shown in Figure 4c, during etching of ZnSe/CdS nanocrystals, the absorption tail at 500−630 nm associated with the interfacial (type II) e−h recombination decreases at a faster rate than the region near 420 nm associated with absorption in ZnSe seeds,

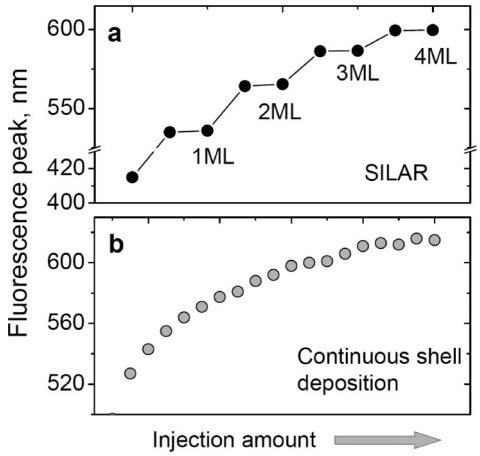


**Figure 5.** Evolution of emission peak during growth of the CdS shell onto 5.2 nm ZnSe cores by (a) SILAR and (b) continuous shell deposition techniques.

indicating a decline in the total area of the ZnSe/CdS interface. This trend becomes apparent if the ratio of absorption at 550 nm to absorption at 420 nm is plotted versus the etching time (Figure 4d). We assume that the complete removal of the CdS shell from ZnSe seeds occurs when this ratio reaches its saturation, which according to Figure 4d takes place in ~120 s. From the known etching rate of CdS of 0.02 nm/s and the measured etching time of ZnSe/CdS nanocrystals, we estimate the shell thickness to be 1.23 nm, which corresponds to 3.5 MLs of CdS.

Probably the most definitive evaluation of the shell thickness in ZnSe/CdS nanocrystals can be obtained through an alternative synthesis via successive layer deposition by SILAR.[24,26] This method relies on the controlled growth of a full CdS ML at a time by consecutive injection of Cd and S precursors, such that the shell thickness during any stage of the synthesis is known. By comparing the shell growth kinetics recorded for continuous and stepwise layer deposition onto 5.2 nm ZnSe seeds, we also estimated the stoichiometric ratio of precursors that form a single ML. In using the SILAR approach, the addition of consecutive MLs caused the emission color of the reaction mixture to change from 535 to 600 nm in a stepwise manner (1 ML: 535 nm, 2 MLs: 566 nm, 3 MLs: 587 nm, and 4 MLs: 600 nm) as shown in Figure 5a. Deposition of the fifth ML did not cause any noticeable red-shift of the emission and was accompanied by a substantial drop in the QY. Through a side-by-side comparison of the spectral evolution of SILAR-synthesized nanocrystals, shown in Figure 5a, to the growth kinetics obtained by continuous addition of precursors (Figure 5b), we estimated the total number of MLs in saturated ZnSe/CdS nanocrystals to be four (shell thickness was 1.4 nm). This result is consistent with shell thickness estimates obtained by BPO etching of ZnSe/CdS QDs emitting at 600 nm. On the basis of the SILAR data, we also determined the number of submonolayers for the intermediate measurements shown in Figure 2. These results compare well with model calculations summarized in Figure 1 (contour plot), predicting that ZnSe/CdS nanocrystals with core sizes of 5.2 nm ($R = 2.6$ nm) would exhibit a type II localization regime for shell thicknesses, $H$, exceeding $H_m = 0.9$ nm (for $R = 2.6$ nm), whereas for $H < H_m$, the electronic localization is transitional from type I to type II. In the present measurements, the amount of type II carrier interactions can be quantified by the intensity of spatially indirect emission across the core/shell. The latter rises with increasing $H$ and reaches its maximum at $\lambda = 588$ nm, corresponding to a shell thickness of 1.05 nm (≈3 ML), which is consistent with the predicted value of $H_m$.

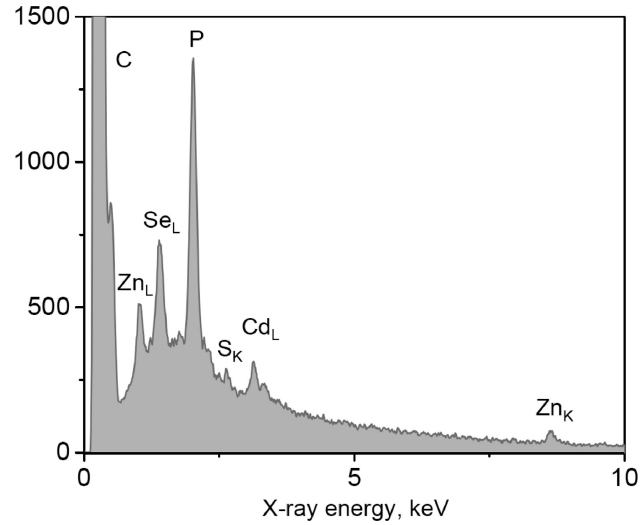


**Figure 6.** Energy dispersive X-ray emission spectrum of ZnSe/CdS nanocrystals with 4 ML of CdS.

**EDX.** Energy dispersive X-ray emission spectra were obtained to further verify the elemental composition of ZnSe/CdS nanocrystals. For this purpose, the hexane suspension of purified ZnSe/CdS QDs with a FL peak at 600 nm was evaporated onto a carbon substrate and loaded into SEM equipped with an X-ray detector. Figure 6 shows a typical X-ray spectrum obtained at 20 kV, along with peak assignments for Zn, Se, Cd, and S elements. After integrating the peak area, the X-ray count was converted into the elemental weight percentages using quantification software (EDAX Genesis). The resulting molar ratio of Cd to Zn was found to be 1.8 ± 0.5, which corresponds to a shell thickness of ~1.1 nm for 5.2 nm ZnSe seeds. This value is 10% lower than the shell thickness estimated by BPO etching and 20% lower than by SILAR, which is likely due to an intrinsic uncertainty associated with nonuniform growth of the shell around ZnSe seeds observed in TEM measurements.

**TEM.** Figure 7 shows TEM images of ZnSe/CdS nanocrystals, fabricated by depositing 2 MLs of CdS onto 4.7 nm ZnSe seeds using the SILAR approach. A nearly spherical shape was observed for most of the examined QDs with the exception of a small fraction of nanocrystals that were slightly elongated. This effect could be attributed to a wurtzite structure of nanocrystal samples, where an oval shape is caused by a faster growing rate of the shell material along the *c*-axis. The diameter of ZnSe/CdS structures was determined by examining several specimens under high-resolution conditions (300 000×). The average nanocrystal size determined in such measurements was 6.0 nm, corresponding to ~1.9 MLs of CdS, which is in good agreement with the intended deposition of 2 ML. Crystalline quality was then studied under ultrahigh-resolution conditions (500 000×) that allow resolving individual lattice planes, as shown in a typical image in Figure 7c. Examination of several specimens revealed a low frequency of stacking faults in the lattice, which appeared to be homogeneous throughout the core/shell structure.

**XPD.** The crystal structure of ZnSe/CdS core/shell nanocrystals was investigated using X-ray powder diffraction of purified samples prepared by overcoated 5.0 nm ZnSe seeds with 4 MLs of CdS. The diffraction pattern shown in Figure 8a predominantly consists of spectral features that correspond to a bulk CdS crystal lattice, with no significant contribution from ZnSe. This serves as additional evidence supporting the core/shell structure of fabricated nanocrystals and indicates that the

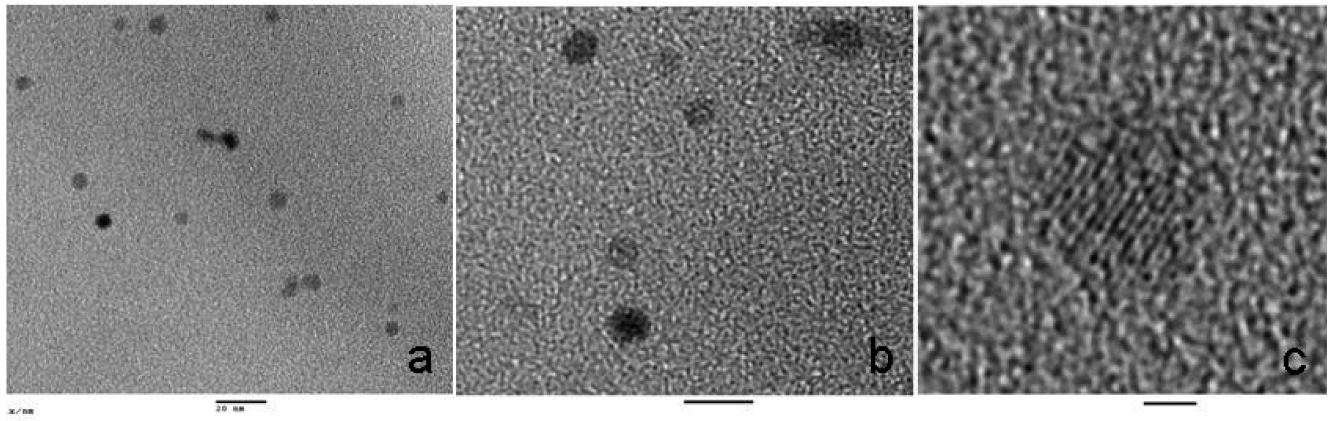


**Figure 7.** High-resolution TEM images of ZnSe/CdS nanocrystals grown from 5.7 nm ZnSe seeds. The scale bars are (a) 20 nm, (b) 10 nm, and (c) 2 nm.

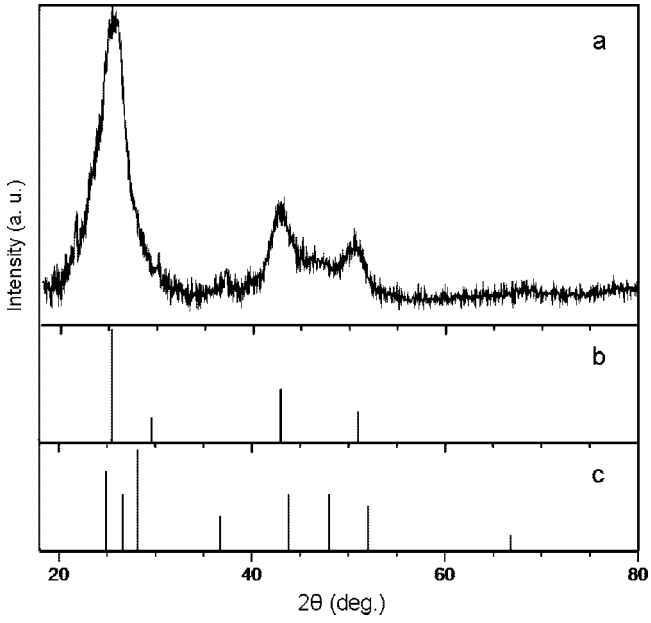


**Figure 8.** (a) Powder X-ray diffraction spectrum of ZnSe/CdS nanocrystals prepared by depositing 4 MLs of CdS on 5.0 nm ZnSe seeds. The peak positions of the sample are compared to the ones of bulk cubic (b) and hexagonal (c) CdS crystal structures. Spectral features corresponding to the bulk ZnSe crystal structure (either wurtzite or zinc blende) were not observed.

shell is deposited on the entire surface of ZnSe and not only in the preferential direction of crystal growth. By comparing the peak positions with the two phases of bulk CdS in Figure 8b,c, we confirm the existence of both hexagonal and cubic lattice types in ZnSe/CdSe nanocrystals. On the basis of measured X-ray diffraction spectra and careful examination of high-resolution TEM images, such as the one in Figure 7c, we also conclude that the wurtzite crystal structure is the primary phase in our samples. The differences in the intensities of the XPD pattern of bulk (Figure 8c) and nanoparticle CdS are attributed to the occasional stacking faults in the nanocrystal lattice.

## Conclusion

Novel type II ZnSe/CdS heteronanocrystals were fabricated via colloidal synthesis by either continuous or stepwise deposition of Cd and S organometallic precursors onto monodisperse ZnSe QDs. The samples were characterized by UV−vis absorption and FL spectroscopy, TEM, energy dispersive X-ray elemental analysis, and X-ray diffractrometry. An efficient charge separation across the interface in ZnSe/CdS nanocrystals was witnessed by a strong PL originating from spatially indirect carrier recombination. By studying the shell growth kinetics, we concluded that the type II regime in ZnSe/CdS was established after the deposition of 3 or more MLs of CdS, which agreed well with our model calculations.

Fabricated ZnSe/CdS nanocrystals possess a combination of interesting properties. For instance, the observed large Stokes shifts, of up 110 nm, can be of use in applications that require a small degree of spectral overlap between emission and absorption profiles such as in Föster resonant energy transfer-based sensors or when reduced self-absorption of colloids is an advantage. Furthermore, the charge separation in ZnSe/CdS results in the shell localization of excited electrons, which can be utilized in dye sensitized solar cells, as it increases the rate of electron transfer from a sensitizer (nanocrystal) to a wide band gap semiconductor ($TiO_2$, ZnO). Finally, the emission wavelength of fabricated nanocrystals is tunable in a wide spectral range, which is an important property for type II heterostructures due to their potential use in hybrid LED and lasing applications.

**Acknowledgment.** The authors thank Prof. D. C. Neckers and R. Adhikari for their help with synthetic procedures and optical measurements.

## References and Notes

(1) Zhang, Y.; Wang, L. W.; Mascarenhas, A. *Nano Lett.* **2007**, *7*, 1264.
(2) Luque, A.; Marti, A.; Nozik, A. J. *MRS Bull.* **2007**, *32*, 236.
(3) Klimov, V. I. *Annu. Rev. Phys. Chem.* **2007**, *58*, 635.
(4) Medintz, I. L.; Uyeda, H. T.; Goldman, E. R.; Mattoussi, H. *Nat. Mater.* **2005**, *4*, 435.
(5) Doose, S. *Small* **2007**, *11*, 1856.
(6) Klimov, V. I.; Ivanov, S. A.; Nanda, J.; Achermann, M.; Bezel, I.; McGuire, J. A.; Piryatinski, A. *Nature (London, U.K.)* **2007**, *447*, 441.
(7) Chan, Y.; Steckel, J. S.; Snee, P. T.; Caruge, J. M.; Hodgkiss, J. M.; Nocera, D. G.; Bawendi, M. G. *Appl. Phys. Lett.* **2005**, *86*, 73102.
(8) Kim, S.; Fisher, B.; Eisler, H. J.; Bawendi, M. *J. Am. Chem. Soc.* **2003**, *125*, 11466.
(9) Schöps, O.; Le Thomas, N.; Woggon, U.; Artemyev, M. V. *J. Phys. Chem. B* **2006**, *110*, 2074.
(10) Yu, K.; Zaman, B.; Romanova, S.; Wang, D.; Ripmeester, J. *Small* **2005**, *1*, 332.
(11) Xie, R.; Zhong, X.; Basché, T. *Adv. Mater.* **2005**, *17*, 2741.
(12) Cheng, C. T.; Chen, C. Y.; Lai, C. W.; Liu, W. H.; Pu, S. C.; Chou, P. T.; Chou, Y. H.; Chiu, H. T. *J. Mater. Chem.* **2005**, *15*, 3409.
(13) Danek, M.; Jensen, K. F.; Murray, C. B.; Bawendi, M. G. *Chem. Mater.* **1996**, *8*, 173.
(14) Ivanov, S. A.; Nanda, J.; Piryatinski, A.; Achermann, M.; Balet, L. P.; Bezel, I. V.; Anikeeva, P. O.; Tretiak, S.; Klimov, V. I. *J. Phys. Chem. B* **2004**, *108*, 10625.

(15) Ivanov, S. A.; Piryatinski, A.; Nanda, J.; Tretiak, S.; Zavadil, K. R.; Wallace, W. O.; Werder, D.; Klimov, V. I. *J. Am. Chem. Soc.* **2007**, *129*, 11708.

(16) Pandey, A.; Guyot-Sionnest, P. *J. Phys. Chem. B* **2007**, *127*, 104710.

(17) Reiss, P. *New J. Chem.* **2007**, *31*, 1843.

(18) Piryatinski, A.; Ivanov, S. A.; Tretiak, S.; Klimov, I. V. *Nano Lett.* **2007**, *7*, 108.

(19) Reiss, P.; Quemard, G.; Carayon, S.; Bleuse, J.; Chandezon, F.; Pron, A. *Chem. Mater.* **2004**, *84*, 10.

(20) Yu, W. W.; Qu, L.; Guo, W.; Peng, X. *Chem. Mater.* **2003**, *15*, 2854.

(21) Battaglia, D.; Blackman, B.; Peng, X. G. *J. Am. Chem. Soc.* **2005**, *127*, 10889.

(22) *Landolt-Boernstein: Numerical Data and Functional Relationships in Science and Technology. Group III, Condensed Matter, Sub Volume C*; Martienssen, W., Ed.; Springer Verlag: Berlin, 1998.

(23) Dinger, A.; Petillon, S.; Grü n, M.; Hetterich, M.; Klingshirn, C. *Semicond. Sci. Technol.* **1999**, *14*, 595.

(24) Li, J. J.; Wang, Y. A.; Guo, W.; Keay, C. J.; Mishima, D. T.; Johnson, B. M.; Peng, X. *J. Am. Chem. Soc.* **2003**, *125*, 12567.

(25) Yu, W. W.; Qu, L.; Guo, W.; Peng, X. *Chem. Mater.* **2003**, *15*, 2854.

(26) Park, S.; Clark, B. L.; Keszler, D. A.; Bender, J. P.; Wager, J. F.; Reynolds, T. A.; Herman, G. S. *Science (Washington, DC, U.S.)* **2002**, *297*, 65.

JP801523M